Environmental application of engineering magnesite slag for phosphate adsorption from wastewater

Hai Liang (lianghai@yku.edu.cn)
Yingkou Institute of Technology https://orcid.org/0000-0001-6983-7165
Panliang Guo
Yingkou Institute of Technology
Yunhong Yang
Yingkou magnesite chemical ind group co., ltd.
Wanting Wang
Yingkou Institute of Technology
Zhaonan Sun
Yingkou Institute of Technology

Research Article

Keywords: Phosphate removal, Magnesite slags, Adsorption, Isotherm, Kinetics

Posted Date: January 20th, 2022

DOI: https://doi.org/10.21203/rs.3.rs-1215339/v1

Version of Record: A version of this preprint was published at Environmental Science and Pollution Research on April 6th, 2022. See the published version at https://doi.org/10.1007/s11356-022-20029-z.

Abstract

Herein, magnesite slags (MS), which remain after sulfuric acid extraction from light burnt magnesite in the magnesite industry, were used as phosphate adsorbents in wastewater. The MS were calcined under 700°C to enhance phosphate adsorption. The calcined magnesite slags (CMS) were characterized by nitrogen adsorption-desorption isotherm, X-ray diffraction and scanning electron microscopy. A series of batch adsorption experiments were carried out to test the phosphate adsorption capacity of CMS. The results showed that the calcific treatment promoted the conversion from Mg, Ca, Fe, etc. compound to metal oxide of the MS. The generated metal oxide particles resulted in 237.4 mg/g increase in the phosphate adsorption capacity. The phosphate adsorption isotherm of CMS fitted the Langmuir model better, the maximum adsorption capacity of CMS was 526 mg/g. The adsorption kinetics of phosphate on CMS can be described by the pseudo-second-order model. The phosphate removal efficiency was greater than 98% in 300 mg/L phosphate solution. The results obtained in this work demonstrate that the CMS is a potential effective adsorbent for removal and reutilization phosphate from P-contaminated water, due to it can be employed as a fertilizer after phosphate adsorption.

1. Introduction

Phosphorus is an essential macronutrient for the growth of plant. However, agriculture and industry activities have produced excessive phosphorus, the releasing of phosphorus into surface water such as rivers, lakes may lead to environmental eutrophication which is threating the ecological balance and human body health(Conley et al. 2009, Huisman et al. 2018, Morelli et al. 2018, Resiere et al. 2018). Phosphorus is a nonrenewable resource on earth, the reserves phosphorus ores on earth are proved to be exhausted without intervention measures(Tang et al. 2017). In addition, phosphorus is an important element for global food security with a highly dissipative (Scholz &Wellmer 2013). It is imperative to develop an effective technology to remove and reutilize phosphorus from P-contaminated water(Li et al. 2018, Zhang et al. 2021b).

Tremendous methods have been developed to remove phosphate such as chemical precipitation, biological treatment, membrane separation and adsorption. previous studies have revealed that phosphorus adsorption is and effective technology to capture and reutilize phosphorus from wastewater(Li et al. 2016a). Several mineral slags such as dolomite, bentonite, calcite and sepiolite waste minerals have been developed as phosphorus adsorbents from wastewater, due to their stability, high affinity of phosphate and richness in macronutrient for plant (Mg, Fe, Ca, etc.). The mineral adsorbent has a potential application as a slow-release fertilizer after phosphate adsorption (Li et al. 2020, Li et al. 2016b, Tang et al. 2018, Yao et al. 2013).

The magnesite slag is a by-product generated in the acid treating process of light burnt magnesite. In 2020, around 3 million tons of $MgSO_4{\cdot}H_2O$, $MgSO_4{\cdot}7H_2O$ and other magnesium salt had been produced from magnesite in China, whereas, the by-production of MS was around 50000 tons which cannot be completely consumed. The main composition of MS is magnesium carbonate, basic magnesium sulfate,

silica, calcium carbonate, ferric oxide, aluminium oxide, etc. Many researchers have develop several mineral slag(blast furnace slag(Guo et al. 2017), ferromanganese slag(Jain &Maiti 2021), electric arc furnace slag(Liu et al. 2020), ferrous slag and carbon steel slag(Zheng et al. 2020)) as efficient adsorbent based on its physical and chemical properties. However, there is some lack of exploitation about efficient adsorbent of MS.

In this study, MS was activated by calcination process. The aim of this work was to develop a phosphate adsorbent from MS for the recovery of phosphate from aqueous solution. Specially, solution pH, adsorption isotherm and kinetics of were investigated with batch experiments, subsequently the efficiency of phosphate-contained adsorbent as a fertilizer were examined.

2. Materials And Methods

2.1. Materials

Magnesite slags (MS) used in the experiments is a magnesite waste generated in the H_2SO_4 treating process of light burnt magnesite obtained from Yingkou Magnesite Chemical Ind Group CO., LTD. CHINA. The MS was washed by purified water three times to minimize the presence of solvend, then dried, smashed and sieved, the MS powder with a particle size between 80-100 mesh was collected for use. Monopotassium phosphate (KH_2PO_4), hydrochloric acid (HCl), sodium hydroxide (NaOH), and other analytical chemical reagents of analytical grade were purchased from Aladdin Industrial Corporation. Purified water was employed to prepare aqueous solutions.

2.2 Calcined magnesite slag preparation

The raw MS were transferred into a muffle furnace and calcined at 10°C/min up to 700°C for 2h. After cooling down to the room temperature, the calcined magnesite slags (CMS) were sealed in a desiccator for further experiment tests. To investigate the effect of calcination temperature on the transformation of MS, calcined magnesite slags (CMS) prepared at 600, 700 and 800°C were expressed as CMS 600, CMS 700, and CMS 800 respectively. As a contrast, magnesite slags (80-100 mesh) without calcination was tested.

2.3 Calcined magnesite slag characterization

The main elemental composition of the MS determined by X-ray fluorescence (XRF, S4 Pioneer, Bruker AXS, Germany) were summarized in Table 1, the raw MS mainly consisted of Mg, Si, S, Ca, Fe, Al and other elements. The surface morphology and elements of the CMS were analyzed by scanning electron microscopy (SEM) and energy dispersive spectrometer (EDS) (FESEM-EDS, S-4800, Hitachi, Japan). The crystallographic structure of CMS was characterized by X-ray diffractometry (XRD, D8 Advance Sol-X, Bruker Co., USA), the samples were scanned in a 2 theta 5-85°. The BET specific surface area, total pore volume and average pore diameter of the MS and CMS were characterized by nitrogen adsorption-

desorption isotherms at 77 K on automated adsorption equipment (BSD-PM2, Beishide instrument, China).

Table 1
Composition of the MS (mass %).

Mg	Si	S	Ca	Fe	Al
13.177	6.234	5.192	4.445	1.391	1.021

2.4 Phosphate adsorption experiments

Batch adsorption experiments were performed to obtain the phosphate adsorption behavior of CMS. Firstly, phosphate stock solutions were prepared by dissolving a certain amount of KH_2PO_4 in deionized water to get an initial concentration of 1000 mg L^{-1}. For adsorption isotherm experiment 0.1 g CMS were accurately weighed and placed in a stoppered 250 mL conical flask and 100 mL of different initial phosphate concentrations (50, 100, 150, 200, 250, 300, 350, 400, 450 and 500 mg L^{-1}, respectively) were mixed in the conical flask. Then the mixtures were shaken at 180 rpm in a 25°C air bath for 24h. After adsorption, the supernatant was separated by filtering through a 0.45 μm microfiltration membrane for phosphate concentration analysis. Phosphate concentrations in solutions before and after adsorption were analyzed by the molybdenum blue method with a UV-Vis spectrophotometer (UV1900, Shimadzu, Japan). The absorbance was determined at a wavelength of 880 nm and according to absorbance of the samples that calculate the equilibrium concentration of phosphate. equilibrium phosphate adsorption capacities q_e (mg-P g^{-1}) were calculated by the mass balance as expressed in Eq. (1).

$q_e=V(C_0-C_e)/m$ (1)

Where C_0 is the initial phosphate concentration (mg L^{-1}), C_e is the equilibrium phosphate concentration (mg L^{-1}), V is the volume of phosphate solution(L), and m is the adsorbent mass (g).

The adsorbed amount of phosphate analyzed with two isotherm equations: Langmuir and Freundlich models, which expressed as follows:

Langmuir. $q_e=q_mK_LC_e/(1+K_LC_e)$ (2)

Freundlich. $q_e=K_FC_e^{1/n}$ (3)

where K_L and K_F, are the constants of Langmuir and Freundlich, respectively. q_m is the maximum adsorption capacity of the adsorbent, n is the heterogeneity factor.

Kinetics of phosphate adsorption on CMS were determined by performing batch adsorption experiments. Mixing a series of 0.5 g CMS with 100 mL phosphate solutions (initial pH=9, 300 mg L^{-1} phosphate diluted from phosphate stock solution). The mixtures were shaken at 25°C, 180 rpm, filtered at selected

time intervals. The phosphate concentration of the filtrates was analyzed as described above. Pseudo-first-order and pseudo-second-order models were used to illustrate the adsorption mechanism of CMS.

Pseudo-first-order. $q_t=q_e(1-\exp(-K_{p1}t))$ (4)

Pseudo-second-order. $q_t=K_{p2}q_e^2t/(1+k_{p2}q_et)$ (5)

where K_{p1} and K_{p2}, are the pseudo-first-order and pseudo-second-order rate constants, respectively. q_e and q_t are the phosphate adsorption amount of the adsorbent at equilibrium and time t, respectively

3. Results And Discussion

3.1 Physical and chemical properties of CMS

The XRD spectra of MS samples (Fig. 1) demonstrated the presence of $MgCO_3$ (JCPDS card No. 08-0479), $Mg_3(OH)_4SO_4·8H_2O$ (No. 53-1039), SiO_2 (No. 75-0443), etc., the XRD analysis revealed that the composition of MS was consistent with that result of XRF. After calcination, The XRD spectra of CMS peaks indicated the formation of MgO particles from $MgCO_3$, $Mg_3(OH)_4SO_4·8H_2O$ during pyrolysis, SiO_2 (No. 75-0443) was also observed as the which remains from the raw magnesite waste. The highly dispersed MgO particles on CMS was ascribed to the dehydrogenation and decomposition of $MgCO_3$, $Mg_3(OH)_4SO_4·8H_2O$ compounds(Choudhary et al. 1992), which could provide efficient adsorption site for phosphate in water(Jiang et al. 2019, Luo et al. 2021).

Understanding the calcination processes of MS was crucial for insight into the active site formation of material. The calcination behavior of CMS generated from MS was analyzed by TGA-DTA (5°C/min to 800°C). As depicted in Fig. 2, the turning temperature points indicated different stages of MS decomposition, the first step ranged from room temperature to 120°C was ascribed to the loss of water and volatiles from the MS(Luo et al. 2021). The second step varied from 120 to 318°C was the dissociation of crystal water. The third stage within the range of 318 to 451°C was attributed to the decomposition of hydroxyl(Wang et al. 2020). The fourth stage ranged from 451 to 681°C was the conversion of carbonate into CO_2.The decomposition of MS during the thermal treatment, as shown in the following reaction.

$Mg_3(OH)_4SO_4·8H_2O→MgO+SO_3+H_2O$

$MgCO_3·nH_2O→MgO+CO_2+H_2O$

$MgSO_4→MgO+SO_3$

$MgCO_3→MgO+CO_2$

The morphology and microstructure of the MS and CMS were processed using SEM, EDS(Fig. 3). The SEM proved that the morphology between MS and CMS was significantly different. As shown in Fig. 3a, the SEM image of MS showed irregular plates with a smooth surface, as well as sharp edges and corners. Fig. 3b shows in-situ generated homogeneous nano metal oxide particles on the surface of CMS, the obtained nano particles provided more adsorption sites, and improve phosphate adsorption capacity.

The elemental contents of pristine MS and CMS were analyzed by EDS (Fig. 4c, 4d), the EDS analysis showed the amounts of Mg, O, Ca, Si, Al and Fe elements in the composites. As would be expected, the O% in the CMS decreased, and the Mg, Si, Ca, Al% increased after calcination.

It is well known that Mg, Ca, Fe and Al have a high chemical affinity to phosphate. The MgO, as one of main components of CMS can easily react with phosphate to form Mg-PO_4($Mg_3(PO_4)_2$, $Mg(H_2PO_4)_2$, $MgHPO_4$) composition via precipitation reaction(Liu et al. 2019). The CaO, Fe_2O_3 and Al_2O_3 can react with phosphate ions to form Fe–O–P, Al-O-P complexes by surface complexation(Liu et al. 2019, Peng et al. 2019). Therefore, the CMS used in this work contains MgO, CaO and Fe_2O_3 was promising for phosphate removal from wastewater.

Table 2 lists the porosity-related characteristics (e.g., BET surface area, pore volume, and average pore diameter) of MS and CMS. The MS and CMS were classified as type II isotherms (Fig. 5) with distinct hysteresis loop according to the International Union of Pure and Applied Chemistry classification. Compared to raw MS (specific surface area 4.69 $m^2\ g^{-1}$, total pore volume 0.0315 $cm^3\ g^{-1}$), CMS featured triflingly increased textural properties (specific surface area of 4.73 $m^2\ g^{-1}$ and total pore volume of 0.0356 $cm^3\ g^{-1}$). The specific surface area, total pore volume and average pore diameter of the MS and CMS were approximately similar. The BET data suggested that the in-situ generated metal oxide particles did not impact the specific surface area of CMS.

Table 2
Surface area and pore structure of the MS and CMS.

Sample	S_{BET}($m^2\ g^{-1}$)	V_{Total} ($cm^3\ g^{-1}$)	Average pore width (nm)
MS	4.69	0.0315	26.87
CMS	4.73	0.0356	30.1

3.2 Impact of calcination temperature on phosphate adsorption capacity

The effects of calcination temperature on phosphate adsorption capacity were shown in Fig. 6. With an increase in the calcination temperature from 600°C to 800°C, the SEM figures indicate that a visible increase of nano particles formation on the surface of the CMS. The phosphate adsorption capacity of CMS increases rapidly with the increase of calcination temperature, and then slight decrease when the calcination temperature exceeded 700°C, the phosphate adsorption capacity was 296.9 mg g^{-1}(59.5 mg

g^{-1} of MS). The calcined magnesite slag exhibited much higher adsorption capacity than the pristine magnesite slag. It is mainly because that the high-temperature calcination process could in-situ generate metal oxide particles on the magnesite slag surfaces, which can significantly increase the affinity to phosphate in solution. Thus, the calcination treatment can effectively enhance the phosphate adsorption activity and capacity of magnesite slag, Considering the adsorption amounts and related economic aspects of CMS, CMS-700 was selected for further investigation.

3.3 Impact of pH on phosphate adsorption capacity

The solution pH strongly influenced the adsorption capacity of adsorbent in adsorption process(Zheng et al. 2020). In this work, the effects of pH on phosphate adsorption capacity of CMS were determined by adsorption isotherms, the obtained equilibriums data were fitted by using Langmuir(Eq. 2) and Freundlich(Eq. 3) isotherm models(Fig. 7), the adsorption isotherm parameters were presented in Table 3, as compared to the regression coefficient(R^2), the Langmuir adsorption model showed more satisfactory fitting to the phosphate adsorption isotherms on CMS, which indicated that phosphate adsorbed on CMS is primarily monolayer adsorption. With the increase of pH from 5 to 11, the phosphate adsorption capacity increased, then slight decrease. When the pH value was 9, the highest phosphate capacity for CMS was 526 mg/g, similar results had been reported by other studies(Liu et al. 2020, Luo et al. 2021, Xu et al. 2018, Yang et al. 2014). Thus, CMS had a wide range of pH values from 5~11, alkaline wastewater was more favorable for the phosphate adsorption process. Some studies reported that the main existent of phosphate was $H_2PO_4^-$ and HPO_4^{2-} ions at pH 9 value. The MgO and other metal oxide can generate electrostatic attraction with $H_2PO_4^-$ and HPO_4^{2-} at alkaline environment(Deng et al. 2020).

Table 3
Adsorption isotherms constants for phosphate adsorption onto CMS 700 by different pH of solution.

pH	Langmuir model			Freundlich model		
	K ($L\ mg^{-1}$)	q_m ($mg\ g^{-1}$)	R^2	K_f	n	R^2
5	0.255	410.6	0.96	147.4	4.5	0.85
7	0.196	430.6	0.98	128.7	3.76	0.87
9	0.114	526	0.99	105.2	2.61	0.97
11	0.16	519.8	0.97	146.8	3.53	0.94

3.4 Impact of initial concentration on phosphate adsorption capacity

The effect of initial concentration on phosphate adsorption of CMS was presented in Fig. 8. The results indicated that the adsorption capacity was affected by phosphate concentration. As the initial phosphate

concentration ranging from 50 to 550 mg L^{-1}, the phosphate adsorption capacity on CMS increased significantly. Test with initial phosphate concentration of 50 mg/L showed 99% removal efficiency on CMS. However, the phosphate removal efficiencies were still greater than 90% when the solution concentration was 500 mg L^{-1}. The decrease of phosphate removal efficiency combined with the increase of adsorption capacity with increasing initial phosphate concentrations has been reported(Blanco et al. 2016, Gan et al. 2015).

3.5 Impact of adsorption time on phosphate adsorption capacity

The changes in phosphate removal efficiency and adsorption amount with different adsorption time was presented in Fig. 9a and b. The phosphate removal efficiency and adsorption amount increased with time, and reached equilibrium after 25 min approximately. Nearly 64% and 90% of phosphate was removed within 5 min and 15 min, respectively. The CMS reached the maximum adsorption efficiency of 98.3% after 55 min. To better understand the adsorption mechanism and kinetics of CMS, kinetics modeling of adsorption helps to characterize the adsorption process. The pseudo-first order (Eq. 4) and pseudo-second order (Eq. 5) rate equations were used to model phosphate adsorption on CMS. The fitting results of the adsorption experimental data were represented in Fig. 9b and Table 4. The pseudo-second order better described the adsorption process, which was consistent with other reported works(Cui et al. 2020, Zhang et al. 2021a). The adsorption of phosphate on CMS was dominated by chemical interaction with adsorbate.

Table 4
Kinetics model parameters obtained from phosphate adsorption.

Kinetics model	Parameters	CMS
Pseudo-first-order	q_{cal} (g mg^{-1})	65.27
	k_1 (h^{-1})	0.264
	R^2	0.97
Pseudo-second-order	q_e (g mg^{-1})	71.17
	k_2 (g mg^{-1} h^{-1})	0.006
	R^2	0.99

3.6 Plant growth as a response to P fertilizer applications

To assess the possible utilization of CMS-P as a fertilizer. The CMS-loaded phosphate (CMS-P) was employed as a phosphate-contained fertilizer for agriculture. 0.5 g/kg and 1.0 g/kg of CMS-P was applied to the pot for the treatment, garlic growth was measured after 15 days. As represented in Fig. 10, the

average growth height of garlic seedling above-ground parts in the CMS-P (CMS-P-0.5 (42 cm), CMS-P-1 (44 cm)) was higher than those in the control (30 cm). These results clearly demonstrated that the CMS-P has the potential application of substitute for phosphate fertilizers.

Conclusions

In this work, magnesite slags from the engineering waste of acid extraction of light burnt magnesite were used to prepare phosphate adsorbent by simply calcination process. The calcination process promoted the decomposition of metal compounds impurity and bring active adsorption sites for phosphate. CMS had a wide range of pH values from 5~11, the adsorption capacity of CMS increased with pH value, alkaline wastewater was more favorable for the phosphate adsorption process, Equilibrium adsorption isotherm at pH=9 was fitted by Langmuir, the highest phosphate capacity for CMS was 526 mg/g. The adsorption process conformed to the pseudo-second-order kinetics better. The solid waste after adsorption proved to be a well fertilizer for plant.

Declarations

Acknowledgments We would like to acknowledge the government of Liaoning province, and the Department of Science and Technology for the funding through project Liaoning Revitalization Talents Program (XLYC2007185).

Authors' contributions Hai Liang contributed to the investigation; conceptualization, data curation, writing- Original draft, reviewing and methodology. Panliang Guo, Wanting Wang: performed experiment and data collection. Zhaonan Sun, Yunhong Yang contributed to Editing and Reviewing; All authors read and approved the final manuscript.

Funding This work was supported by grants from the Foundation for Liaoning Revitalization Talents Program (project No. XLYC2007185). Basic scientific research project of colleges and universities of Liaoning education department (project No. LJKZ1202). High-level talents research project of Yingkou Institute of Technology (project No. YJRC202001).

Data availability All data generated or analyzed during this study are available from the corresponding author on reasonable request.

Compliance with ethical standards

Competing interests The authors declare that they have no competing interests.

Ethics approval and consent to participate Not applicable.

Consent for publication Not applicable.

References

1. Blanco I, Molle P, Saenz de Miera LE, Ansola G (2016) Basic Oxygen Furnace steel slag aggregates for phosphorus treatment. Evaluation of its potential use as a substrate in constructed wetlands. Water Res 89:355–365
2. Choudhary V, Pataskar S, Pandit M, Gunjikar V (1992) Influence of precipitation conditions of magnesium hydroxide on its thermal decomposition in the preparation of active MgO. Thermochimica acta 194:361–373
3. Conley DJ, Paerl HW, Howarth RW, Boesch DF, Seitzinger SP (2009) Ecology controlling eutrophication: nitrogen and phosphorus. Science 323:1014–1015
4. Cui Q, Xu J, Wang W, Tan L, Cui Y, Wang T, Li G, She D, Zheng J (2020) Phosphorus recovery by core-shell gamma-Al2O3/Fe3O4 biochar composite from aqueous phosphate solutions. Sci Total Environ 729:138892
5. Deng L, Zhang D, Kong Z, He L, Guan Q, Ning P (2020) Strong immobilization of phosphate in wastewater onto the surface of MgO-modified industrial hemp-stem-driven biochar by flowerlike crystallization. Ind Eng Chem Res 59:14578–14586
6. Gan C, Liu Y, Tan X, Wang S, Zeng G, Zheng B, Li T, Jiang Z, Liu W (2015) Effect of porous zinc–biochar nanocomposites on Cr(vi) adsorption from aqueous solution. RSC Adv 5:35107–35115
7. Guo H, Tang L, Yan B, Wan K, Li P (2017) NaA zeolite derived from blast furnace slag: its application for ammonium removal. Water Sci Technol 76:1140–1149
8. Huisman J, Codd GA, Paerl HW, Ibelings BW, Verspagen JM, Visser PM (2018) Cyanobacterial blooms. Nat Rev Microbiol 16:471–483
9. Jain N, Maiti A (2021) Arsenic adsorbent derived from the ferromanganese slag. Environ Sci Pollut Res Int 28:3230–3242
10. Jiang YH, Li AY, Deng H, Ye CH, Wu YQ, Linmu YD, Hang HL (2019) Characteristics of nitrogen and phosphorus adsorption by Mg-loaded biochar from different feedstocks. Bioresour Technol 276:183–189
11. Li H, Li Y, Xu Y, Lu X (2020) Biochar phosphorus fertilizer effects on soil phosphorus availability. Chemosphere 244:125471
12. Li M, Liu J, Xu Y, Qian G (2016a) Phosphate adsorption on metal oxides and metal hydroxides: A comparative review. Environmental Reviews 24:319–332
13. Li R, Wang JJ, Zhou B, Awasthi MK, Ali A, Zhang Z, Lahori AH, Mahar A (2016b) Recovery of phosphate from aqueous solution by magnesium oxide decorated magnetic biochar and its potential as phosphate-based fertilizer substitute. Bioresour Technol 215:209–214
14. Li R, Wang JJ, Zhang Z, Awasthi MK, Du D, Dang P, Huang Q, Zhang Y, Wang L (2018) Recovery of phosphate and dissolved organic matter from aqueous solution using a novel CaO-MgO hybrid carbon composite and its feasibility in phosphorus recycling. Sci Total Environ 642:526–536
15. Liu J, Jiang J, Aihemaiti A, Meng Y, Yang M, Xu Y, Gao Y, Zou Q, Chen X (2019) Removal of phosphate from aqueous solution using MgO-modified magnetic biochar derived from anaerobic digestion residue. J Environ Manage 250:109438

16. Liu M, Liu X, Wang W, Guo J (2020) : Phosphorus removal from wastewater using electric arc furnace slag aggregate.Environ Technol,1–8
17. Luo H, Wang Y, Wen X, Cheng S, Li J, Lin Q (2021) Key roles of the crystal structures of MgO-biochar nanocomposites for enhancing phosphate adsorption. Sci Total Environ 766:142618–142629
18. Morelli B, Hawkins TR, Niblick B, Henderson AD, Golden HE, Compton JE, Cooter EJ, Bare JC (2018) Critical review of eutrophication models for life cycle assessment. Environ Sci Technol 52:9562–9578
19. Peng Y, Sun Y, Sun R, Zhou Y, Tsang DCW, Chen Q (2019) : Optimizing the synthesis of Fe/Al (Hydr)oxides-Biochars to maximize phosphate removal via response surface model.Journal of Cleaner Production237
20. Resiere D, Valentino R, Nevière R, Banydeen R, Gueye P, Florentin J, Cabié A, Lebrun T, Mégarbane B, Guerrier G (2018) Sargassum seaweed on Caribbean islands: an international public health concern. The Lancet 392:2691
21. Scholz RW, Wellmer F-W (2013) Approaching a dynamic view on the availability of mineral resources: what we may learn from the case of phosphorus? Glob Environ Change 23:11–27
22. Tang X, Wu M, Li R, Wang Z (2017) Prospect of recovering phosphorus in magnesium slag-packed wetland filter. Environ Sci Pollut Res Int 24:22808–22815
23. Tang X, Li R, Wu M, Dong L, Wang Z (2018) Enhanced phosphorus removal using acid-treated magnesium slag particles. Environ Sci Pollut Res Int 25:3860–3871
24. Wang K, Lei H, Muhammad Y, Chen F, Gao F, Wei Y, Fujita T (2020) Controlled preparation of cerium oxide loaded slag-based geopolymer microspheres (CeO2@SGMs) for the adsorptive removal and solidification of F(-) from acidic waste-water. J Hazard Mater 400:123199
25. Xu K, Lin F, Dou X, Zheng M, Tan W, Wang C (2018) Recovery of ammonium and phosphate from urine as value-added fertilizer using wood waste biochar loaded with magnesium oxides. J Clean Prod 187:205–214
26. Yang M, Lin J, Zhan Y, Zhang H (2014) Adsorption of phosphate from water on lake sediments amended with zirconium-modified zeolites in batch mode. Ecol Eng 71:223–233
27. Yao Y, Gao B, Chen J, Yang L (2013) Engineered biochar reclaiming phosphate from aqueous solutions: mechanisms and potential application as a slow-release fertilizer. Environ Sci Technol 47:8700–8708
28. Zhang M, Yang J, Wang H, Lv Q, Xue J (2021a) Enhanced removal of phosphate from aqueous solution using Mg/Fe modified biochar derived from excess activated sludge: removal mechanism and environmental risk. Environ Sci Pollut Res Int 28:16282–16297
29. Zhang X, Gang DD, Sun P, Lian Q, Yao H (2021b) Goethite dispersed corn straw-derived biochar for phosphate recovery from synthetic urine and its potential as a slow-release fertilizer. Chemosphere 262:127861
30. Zheng Q, Zhang Y, Zhang Z, Li H, Wu A, Shi H (2020) Experimental research on various slags as a potential adsorbent for the removal of sulfate from acid mine drainage. J Environ Manage

270:110880

Figures

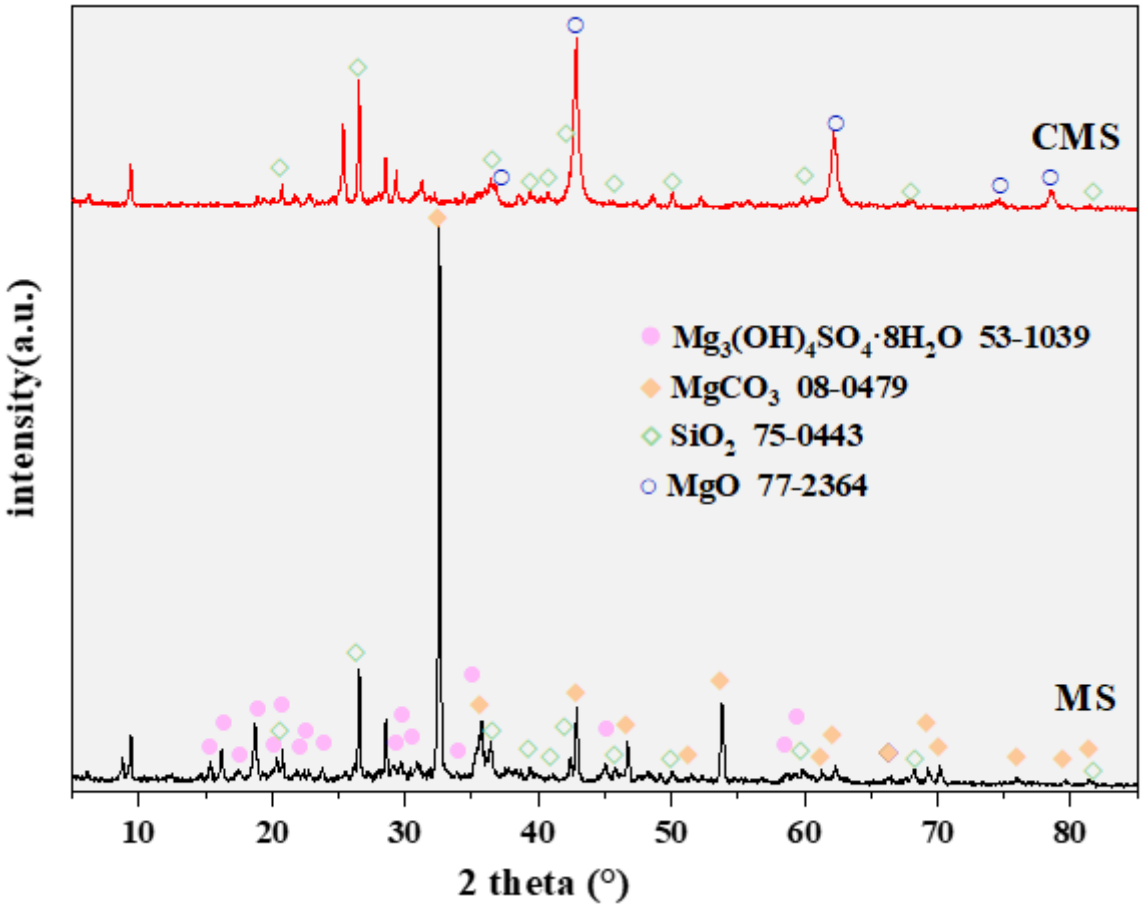

Figure 1

XRD patterns of MS and CMS.

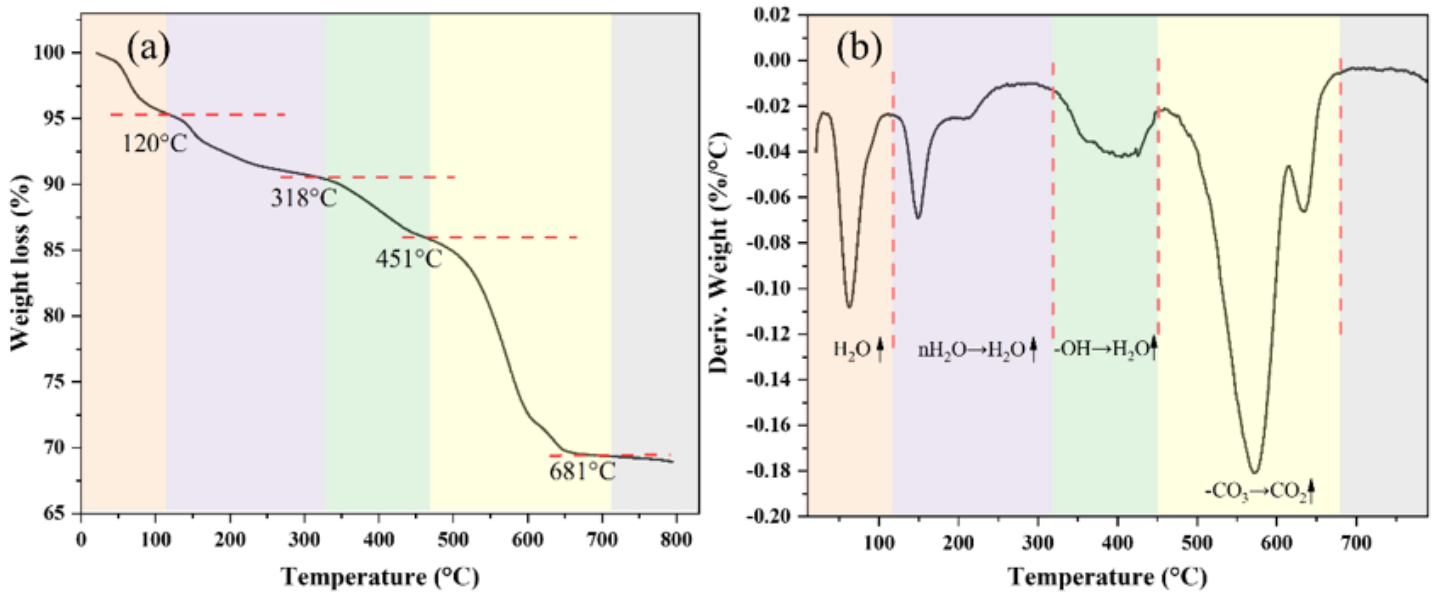

Figure 2

TG(a) and DTA(b) curves of CMS.

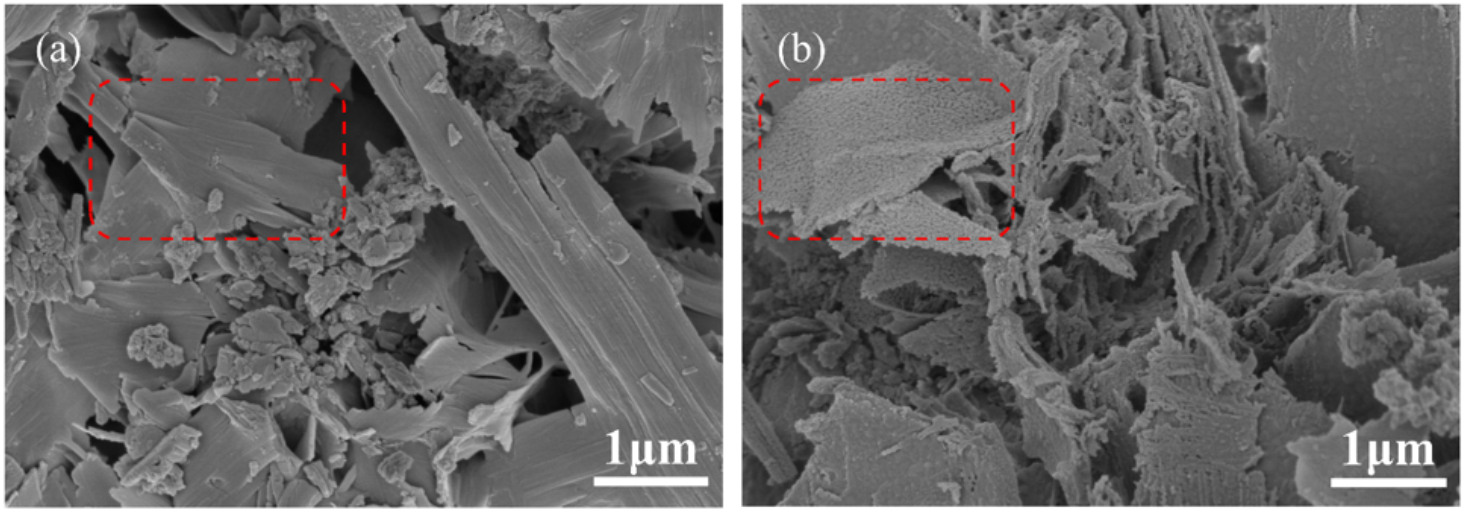

Figure 3

SEM images of (a) MS and (b) CMS.

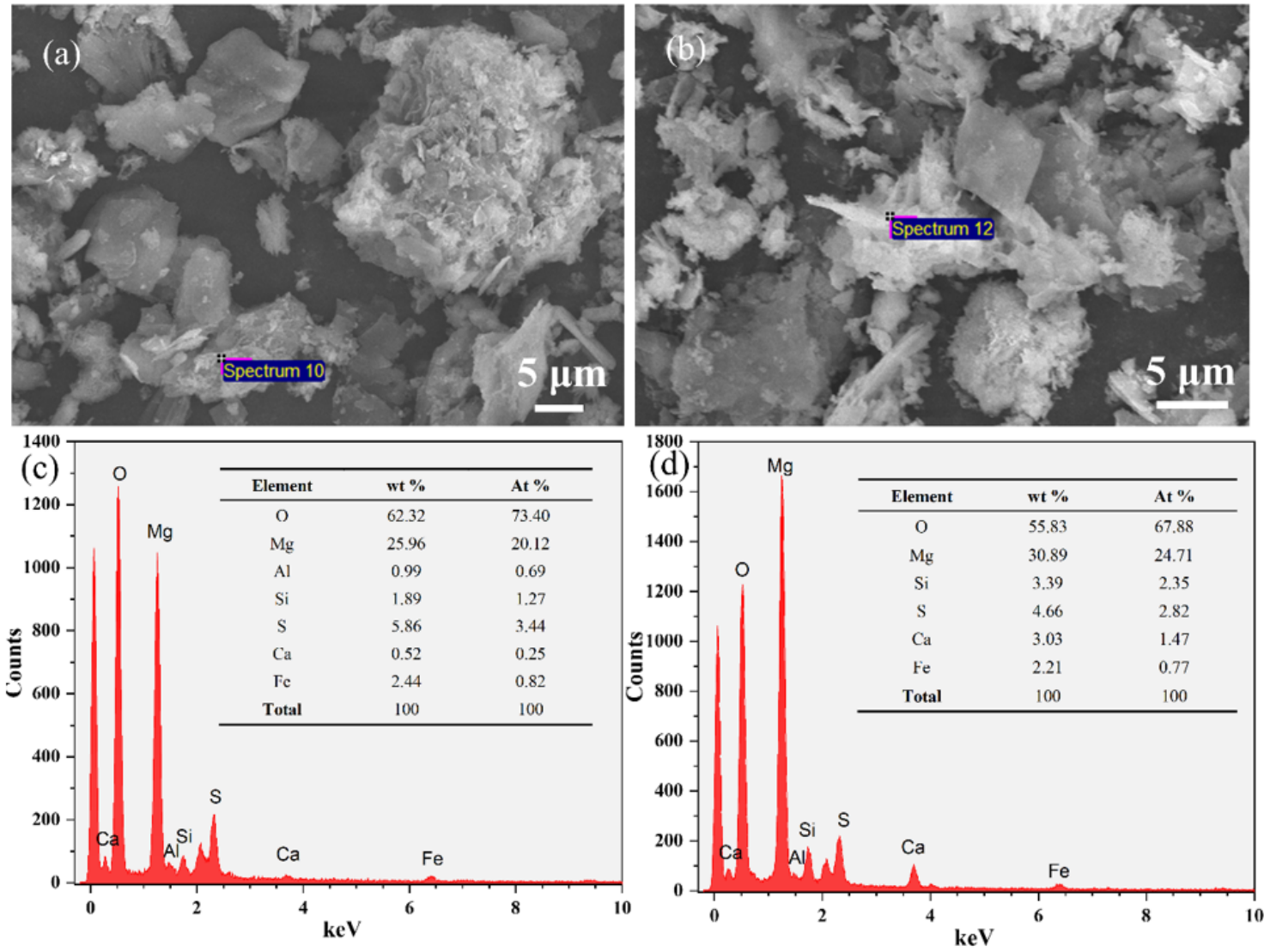

Figure 4

SEM images of (a) MS and (b) CMS, EDS spectrum of (c) MS and (d) CMS, the rectangular in the pictures represent where the EDS was performed.

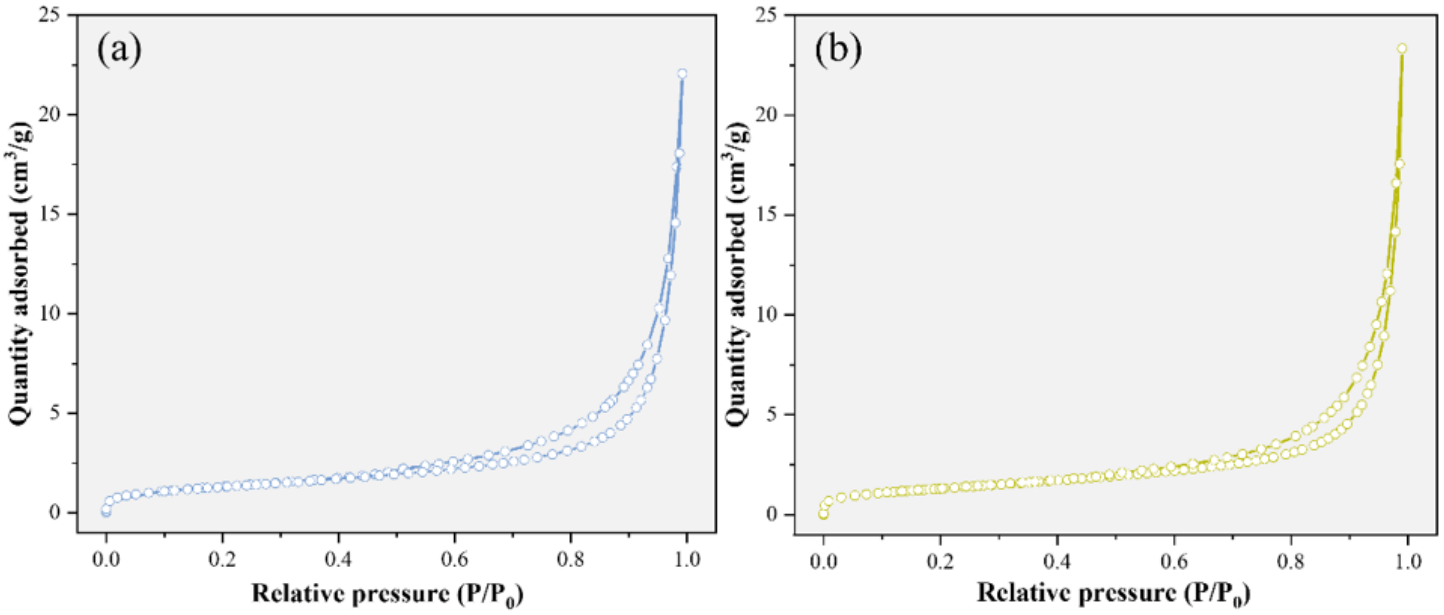

Figure 5

N_2 adsorption-desorption isotherms of (a) MS and (b) CMS.

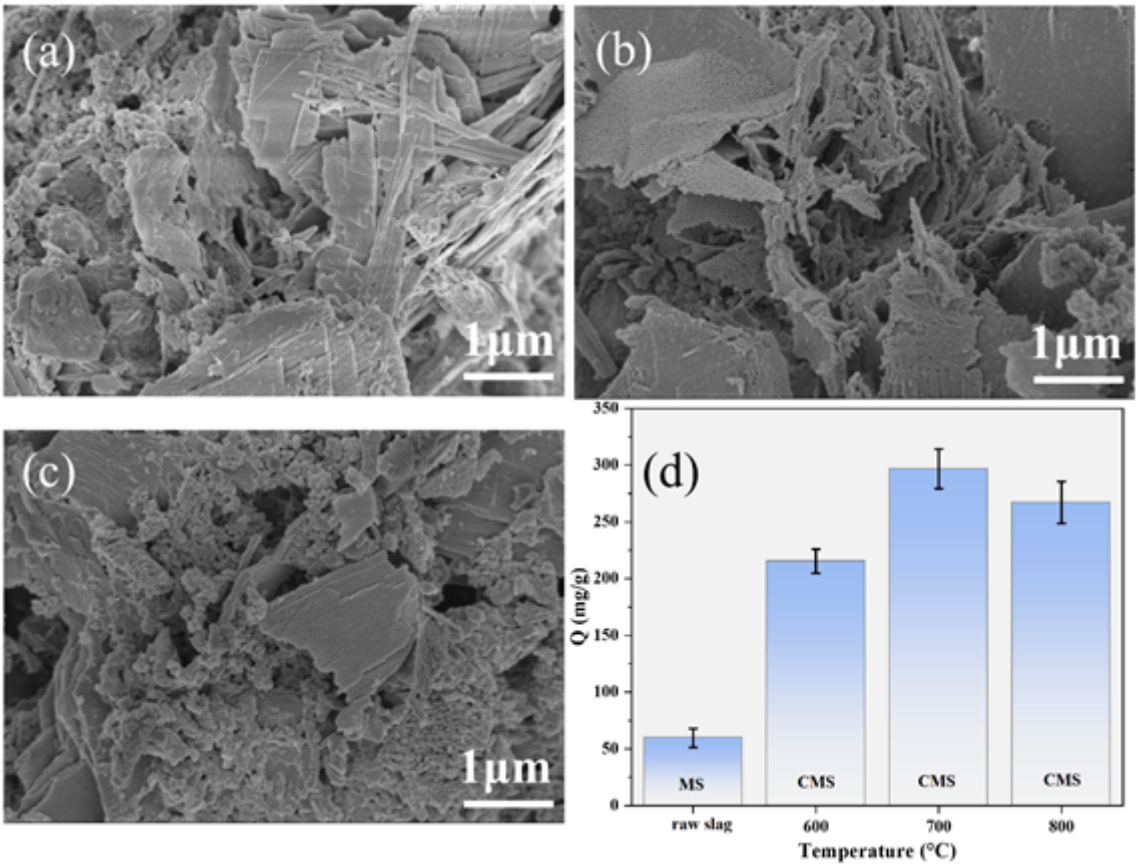

Figure 6

SEM images of CMS at different calcination temperatures (a) CMS 600. (b) CMS 700. (c) CMS 800. (d) phosphate adsorption capacities of MS, CMS 600, CMS 700, CMS 800. phosphate initial concentration =

300 mg L^{-1}, shaking speed = 180 rpm, equilibrium time = 24 h, temperature = 25 °C.

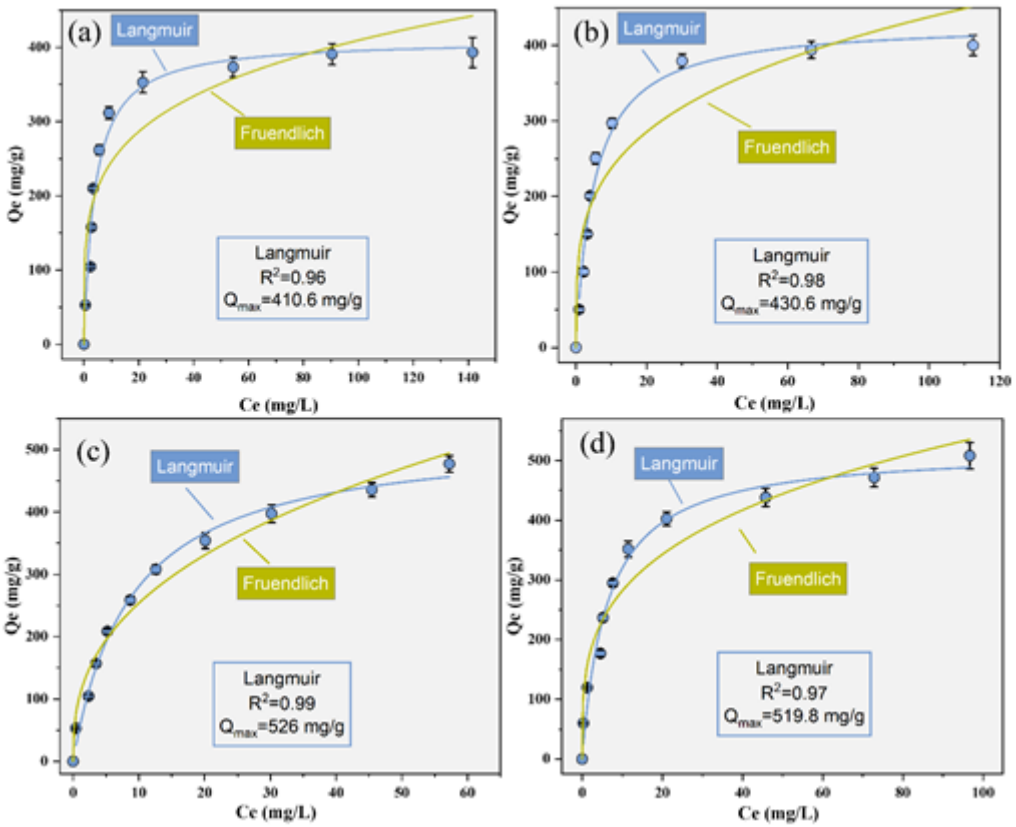

Figure 7

Phosphate adsorption isotherms fitted with Langmuir and Freundlich models of CMS 700((a) pH=5, (b) pH=7, (c) pH=9, (d) pH=11). phosphate initial concentration = 50-500 mg L^{-1}, adsorbent dosage = 1 g L^{-1}, shaking speed = 180 rpm, equilibrium time = 24 h, temperature = 25 °C.

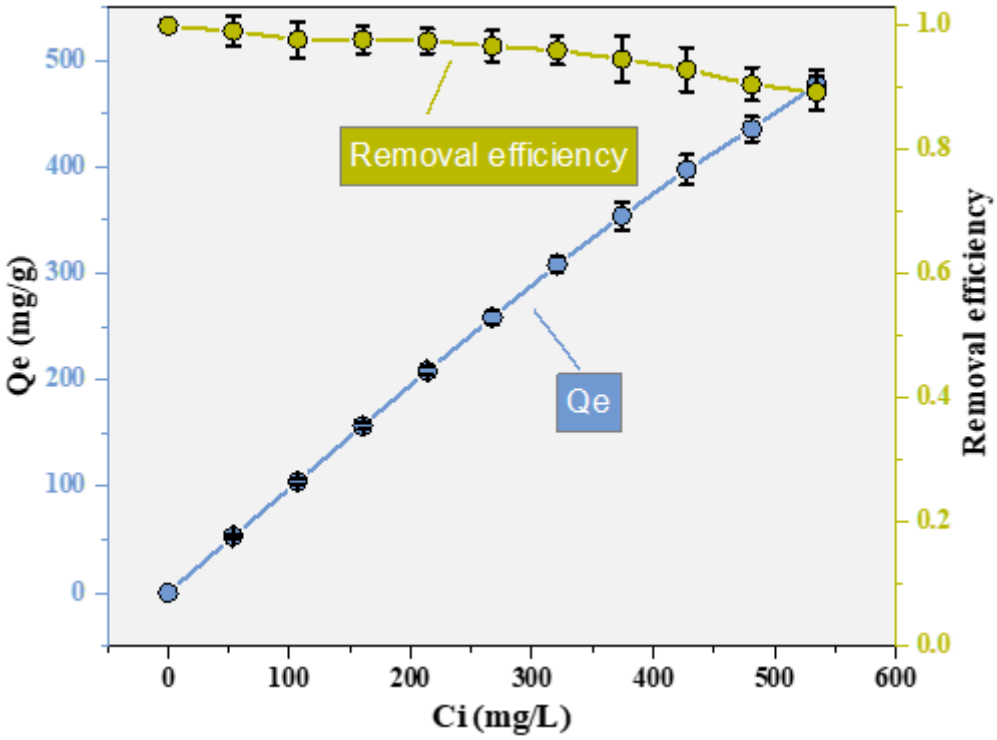

Figure 8

Impact of initial concentration on adsorption capacity (pH=9, adsorbent dosage = 1 g L^{-1}, shaking speed = 180 rpm, temperature = 25 °C).

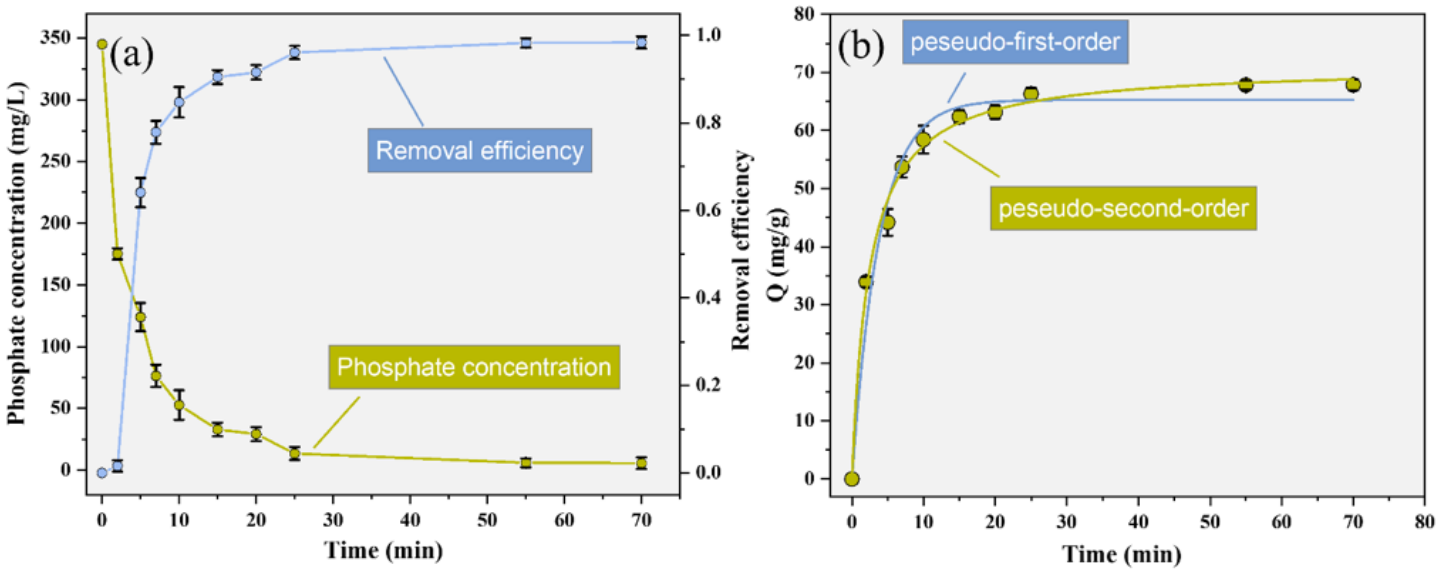

Figure 9

Phosphate adsorption kinetics of CMS 700 (phosphate initial concentration = 300 mg L^{-1}, adsorbent dosage = 5 g L^{-1}, shaking speed = 180 rpm, temperature = 25 °C).

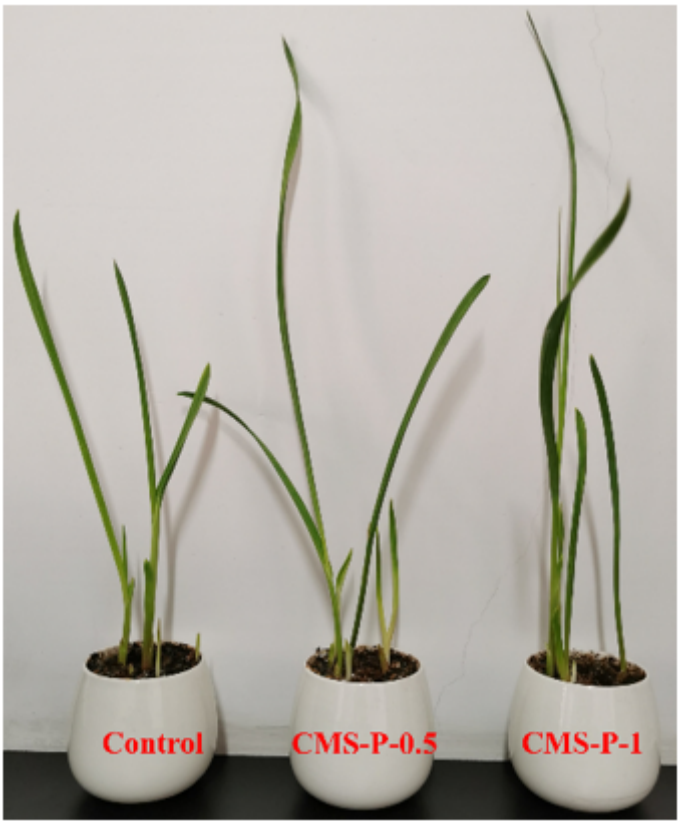

Figure 10

CMS-P application on rice seedling growth of (a) Control (absence of CMS-P), (b) CMS-P-0.5(0.5 g/kg), (c) CMS-P-1(1.0 g/kg).

Supplementary Files

This is a list of supplementary files associated with this preprint. Click to download.

- GraphicalAbstract.png